Meridional Propagation of Planetary-Scale Waves in Vertical Shear: Implication for the Venus Atmosphere

TAKESHI IMAMURA

Institute of Space and Astronautical Science, Japan Aerospace Exploration Agency, Kanagawa, Japan

(Manuscript received 6 September 2004, in final form 26 July 2005)

ABSTRACT

It is shown that planetary-scale waves are inherently accompanied by latitudinal momentum transport when they propagate vertically in vertically sheared zonal flows. Because of the dependence of the wave's latitudinal scale on the intrinsic phase speed, positive (negative) vertical shear should force prograde (retrograde) waves to focus equatorward and retrograde (prograde) waves to expand poleward in the course of upward propagation. Consequently, Eliassen–Palm (EP) flux vectors are tilted from the vertical and nonzero latitudinal momentum fluxes occur. The direction of momentum transport should always be equatorward (poleward) in positive (negative) vertical shear irrespective of the zonal propagation direction.

The idea was applied to upwardly propagating waves in the Venusian middle atmosphere, where vertical shear of strong midlatitude jets and equatorial superrotation exist. Numerical solutions showed that Kelvin and prograde inertio-gravity waves focus equatorward and mixed Rossby–gravity and Rossby waves expand poleward below the cloud top. The former is attributed primarily to the vertical shear of the superrotation, while the latter to the vertical shear beneath the midlatitude jets. Such characteristics of planetary-scale waves will cause angular momentum separation between high and low latitudes and, at least partly, contribute to the maintenance of the superrotation.

1. Introduction

Planetary-scale free waves whose horizontal structures extend over the whole planet have been observed in the middle atmospheres of the Earth, Mars, and Venus (e.g., Andrews et al. 1987; Forbes 2002). The vertical momentum transport by such waves is considered to influence the mean flow and has been studied extensively. Latitudinal eddy momentum flux is zero in the classical wave solutions where the background flow is rigid body rotation; however, the occurrence of such momentum transport in vertically sheared flow has been implied in the studies of equatorial waves, which are the large Lamb-parameter limit of planetary-scale free modes (Longuet-Higgins 1968). Lindzen (1970, 1971) and Holton (1970) investigated via linear theories the properties of equatorial Kelvin and mixed Rossby–gravity waves in vertical shear near critical levels, and showed that both the latitudinal and vertical scales of the waves decrease with height and the vertical momentum transport becomes concentrated toward the equator. Andrews and McIntyre (1976a) obtained asymptotic analytical solutions of those waves in weak vertical and latitudinal shear, and showed that the waves possess latitudinal momentum fluxes.

The influence of background shear on planetary-scale waves might play an important role in the Venusian middle atmosphere, where Kelvin and symmetric Rossby modes with zonal wavenumber 1 are embedded in planetwide sheared flows (e.g., Del Genio and Rossow 1990). The fast rotation of the entire atmosphere may be maintained by the combination of a Hadley circulation and equatorward eddy momentum fluxes (Gierasch 1975). Covey and Schubert (1982) suggested with a linear model that the observed waves are generated as preferred modes of the Venusian atmosphere. The tilt of the phase with latitude in their Rossby wave solution implies equatorward momentum transport, although the authors do not mention it. Smith et al. (1993) also obtained preferred modes in the Venusian atmosphere considering radiative–dynamic cloud feedback, and showed that equatorward momentum fluxes

Corresponding author address: Takeshi Imamura, Institute of Space and Astronautical Science, Japan Aerospace Exploration Agency, 3-1-1, Yoshinodai, Sagamihara, Kanagawa 229-8510, Japan.
E-mail: ima@isas.jaxa.jp

occur in a Kelvin mode. In the Venus-like GCMs by Yamamoto and Takahashi (2003a,b), planetary-scale Rossby and Rossby–gravity waves with wavenumbers 1–2 and gravity waves with larger wavenumbers were observed, and some of them are accompanied by equatorward momentum transport. In the studies above, however, the reason why the planetary-scale free modes are accompanied by latitudinal momentum transport has been unclear. It should be clarified how the background wind influences the wave characteristics and eddy momentum fluxes.

The present study addresses the structures of planetary-scale waves and the meridional momentum transport in sheared zonal flows, with application to the Venusian middle atmosphere. Section 2 describes basic concepts in terms of the equatorial wave theory and the quasigeostrophic dynamics. Section 3 gives numerical solutions of planetary-scale waves in the Venusian middle atmosphere and discusses the properties of waves in sheared flows. Section 4 summarizes the conclusions and discusses implications for the mean-wind acceleration in the Venusian atmosphere.

2. Basic concepts

a. Influence of vertical shear

The energy of any free mode in spherical geometry becomes concentrated toward the equator as the Lamb parameter $4\Omega^2/gh$ increases (Longuet-Higgins 1968), where Ω is the angular velocity of the rigid-body rotation of the background atmosphere in inertial coordinate, g is the gravitational acceleration, and h is the equivalent depth. Since the absolute value of the frequency decreases with the Lamb parameter, the latitudinal scale of any wave increases with the absolute value of the frequency. This tendency holds up to small latitudinal scales (large Lamb parameter); therefore, the tendency should be qualitatively describable on the equatorial β plane. Based on this ground, in this section, such a wave characteristics and the resultant lateral momentum transport are discussed in terms of the equatorial wave theory for simplicity.

Hereafter equations are written in a coordinate system that rotates at a typical angular velocity of the rotation of the entire atmosphere. The latitudinal scale of an equatorially trapped wave is represented by the equatorial deformation radius l_E, which is related to the vertical wavenumber m in the log pressure altitude coordinate z by (Matsuno 1966; Andrews et al. 1987)

$$l_E^2 = \frac{N}{\beta(m^2 + 1/4H^2)^{1/2}}, \tag{1}$$

where N is the buoyancy frequency, β is the meridional derivative of the Coriolis parameter f at the equator, and H is the basic scale height. Here the zonal and meridional coordinates are taken in the direction of planetary rotation and northward, respectively; thus, β is always positive. The wave solutions are classified according to the latitudinal node number n: $n = 0$ gives a mixed Rossby–gravity wave whose intrinsic zonal phase velocity is negative (retrograde) and an inertio-gravity wave whose intrinsic phase velocity is positive (prograde); positive n gives a Rossby wave with retrograde propagation and a pair of inertio-gravity waves with prograde and retrograde propagation; Kelvin wave corresponds to $n = -1$. In this paper, the word prograde denotes the direction of planetary rotation and retrograde denotes the direction opposite to the planetary rotation: prograde is eastward on Earth, while it is westward on Venus.

The l_E depends on the intrinsic frequency ω^* defined by

$$\omega^* = \omega - k\bar{u}, \tag{2}$$

where ω is the frequency, k is the zonal wavenumber, and $\bar{u}$ is the zonal-mean zonal wind velocity. If k is chosen to be positive by convention, ω^* is positive for prograde waves and negative for retrograde waves. Assuming that waves originate in the lower atmosphere and the vertical group velocity is positive; that is,

$$\frac{\partial \omega^*}{\partial m} > 0, \tag{3}$$

it can be shown that $m < 0$ for modes with $\omega^* > 0$ and $m > 0$ for $\omega^* < 0$ (Andrews et al. 1987). The dominance of upwardly propagating waves is a reasonable assumption, if solar energy is injected into the lower atmosphere and waves suffer greater dissipation at higher altitudes. The combination of (1) and (3) yields

$$\frac{\partial l_E}{\partial \omega^*} > 0 \quad \text{for prograde waves,}$$

$$\frac{\partial l_E}{\partial \omega^*} < 0 \quad \text{for retrograde waves.} \tag{4}$$

Figure 1 shows the dependence of the nondimensionalized deformation radius on the nondimensionalized frequency calculated from the dispersion relations for equatorial waves. The dependence is large especially for Rossby and mixed Rossby–gravity waves.

If waves retain their identities in vertically sheared flows and ω^* defined by (2) is replaced with $\omega^*(z)$ at each altitude, l_E should vary with z. In positive shear, that is, $\partial\bar{u}/\partial z > 0$, (2) and (4) imply

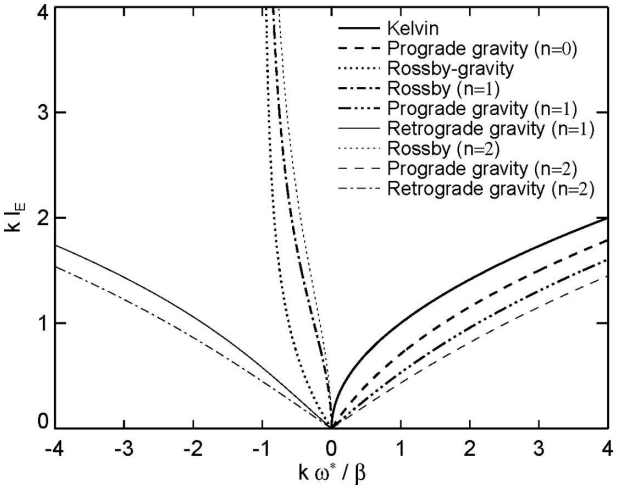

FIG. 1. Relationship between the nondimensionalized deformation radius (kl_E) and intrinsic frequency ($k\omega^*/\beta$) for various equatorial modes.

$$\frac{\partial l_E}{\partial z} < 0 \text{ (focusing)} \qquad \text{for prograde waves,}$$

$$\frac{\partial l_E}{\partial z} > 0 \text{ (defocusing)} \quad \text{for retrograde waves.} \tag{5}$$

The signs of the inequalities are reversed in negative shear. The latitudinal and vertical components of the Eliassen–Palm (EP) flux vector **F** are defined by

$$F^{(\phi)} = \rho_0 a \cos\phi \left(\bar{u}_z \frac{\overline{v'\theta'}}{\bar{\theta}_z} - \overline{v'u'} \right), \tag{6}$$

$$F^{(z)} = \rho_0 a \cos\phi \left\{ \left[f - \frac{(\bar{u}\cos\phi)_\phi}{a\cos\phi} \right] \frac{\overline{v'\theta'}}{\bar{\theta}_z} - \overline{w'u'} \right\}, \tag{7}$$

where ϕ is the latitude; $\rho_0(z)$ is the basic density; a is the planetary radius; u, v, and w the zonal, meridional, and vertical wind velocities, respectively; θ is the potential temperature; the prime ($'$) and overbar ($\bar{}$) denote disturbance and zonal-mean quantities, respectively; and subscripts denote partial derivative. The focusing or defocusing of waves with height should be accompanied by the tilt of EP flux vectors from vertical, since the EP flux divergence should be zero in the absence of dissipation and transience (e.g., Andrews and McIntyre 1976b). Considering that $F^{(z)}$ is negative for prograde waves and positive for retrograde waves, (5) implies that **F** has poleward (equatorward) component in positive (negative) shear irrespective of the zonal propagation direction. In other words, zonal momentum is always transported equatorward (poleward) in positive (negative) shear. Such a momentum transport is consistent with the nature of Kelvin and mixed Rossby–gravity waves suggested by Lindzen (1970, 1971) and Holton (1970). We expect the conclusion is not limited to those two waves but holds for any planetary-scale wave.

In general, $\bar{u}$ is a function of both z and ϕ. Furthermore, the limited latitudinal extent of spherical geometry may have other effects. The exact response of each wave to a given background should be studied with numerical methods.

b. *Influence of latitudinal shear*

Strong vertical shear usually occurs around midlatitude jets, in which the latitudinal structure of $\bar{u}$ is also potentially important. The group propagation of midlatitude Rossby waves with small Rossby number is governed by the distribution of the quasigeostrophic refractive index $n_{k,\omega}$ defined by (Matsuno 1970; Chen and Robinson 1992):

$$n^2_{k,\omega} = \frac{\bar{q}_y}{\bar{u} - \omega\cos\phi/k} - \left(\frac{k}{\cos\phi}\right)^2 - \left(\frac{f}{2NH}\right)^2, \tag{8}$$

where

$$\bar{q}_y = \frac{2\Omega}{a}\cos\phi - \frac{1}{a^2}\left[\frac{(\bar{u}\cos\phi)_\phi}{\cos\phi}\right]_\phi - \frac{f^2}{\rho_0}\left(\rho_0 \frac{\bar{u}_z}{N^2}\right)_z \tag{9}$$

is the meridional gradient of the zonal-mean potential vorticity. We expect waves to propagate in regions where $n^2_{k,\omega} > 0$ and to be deflected up the gradient of $n^2_{k,\omega}$.

Stationary Rossby waves in the terrestrial winter stratosphere tend to be deflected equatorward since $n^2_{k,\omega}$ approaches infinity near the critical surfaces at low latitudes (e.g., Andrews et al. 1987). On the other hand, for planetary-scale waves that do not have critical latitudes, the latitudinal curvature of $\bar{u}$ near midlatitude jets can create $n^2_{k,\omega}$ maxima at high latitudes through $\bar{q}_y$, thereby deflecting upwardly oriented EP flux vectors poleward. Note, however, that it is uncertain to what extent such midlatitude dynamics influences planetary-scale waves.

3. Waves in the Venusian middle atmosphere

The simplified discussion above should be examined with numerical solutions in realistic sheared flows. This section gives numerical solutions of planetary-scale waves in the Venusian middle atmosphere, which provides one of the ideal examples for the physics under consideration. Various planetary-scale waves have been observed in the sheared background flow of the Venusian atmosphere, and the resultant latitudinal mo-

mentum transport may play an important role in the maintenance of the persistent fast zonal circulation.

a. Venusian wind system and observed waves

Venus has a radius of 6050 km, which is similar to that of Earth, and rotates westward with a period of 243 d (d = Earth days). In its massive CO_2 atmosphere, westward wind speed increases with height, and the atmosphere near the cloud top (65–70 km altitude) circles around the planet at a speed of 90–100 m s^{-1} with a period of 4.6–5.0 d (Schubert 1983; Del Genio and Rossow 1990). This wind system, called the superrotation, allows planetary-scale waves to exist in spite of the slow rotation of the planet. Midlatitude jets are also present probably due to the poleward advection of angular momentum by a Hadley circulation. One of the promising mechanisms for maintaining the superrotation is the one proposed by Gierasch (1975): a Hadley circulation, with rising motion near the equator and sinking near the poles, transports angular momentum upward whenever equatorial regions of the atmosphere have angular momentum surplus relative to polar regions.

Various waves have been detected in the cloud brightness field (Del Genio and Rossow 1990); among them are Kelvin waves and gravest symmetric Rossby waves with zonal wavenumber 1. The former occurs near the equator with the latitudinal decay scale of ~20° and the period of 3.9–5.0 d, while the latter occurs at 40°–60° latitudes of both hemispheres with the period of 5.0–6.0 d. Venus-like GCMs predict the occurrence of Rossby, Rossby–gravity, and inertio-gravity waves with wavenumber 1, and larger-wavenumber Kelvin, Rossby, Rossby–gravity, and inertio-gravity waves (Yamamoto and Takahashi 2003a).

Young et al. (1984) argued that the source of the Kelvin and Rossby waves observed can be baroclinic instability in the middle cloud region at 50–60 km altitudes. Unlike terrestrial baroclinic problems, instability will occur only at high altitudes where the vertical curvature of zonal wind is strong, since the superrotation should take the place of planetary rotation. Instabilities will tend to cause disturbances with large deformation radii, that is, planetary-scale eddies, due to the relatively small Coriolis force in the Venusian atmosphere. A nonlinear upward cascade of disturbances, which are forced by convection in the clouds, to larger scales is another possibility (Rossow and Williams 1979; Covey and Schubert 1982).

b. Model description

A nonlinear primitive equation model in spherical geometry covering the Venusian atmosphere from 60 km (236 hPa) to 85 km (2.0 hPa) altitude was developed. Hereafter the altitude means the log-pressure altitude, with H for the temperature at 65 km (245 K). The waves simulated are the four gravest modes: Kelvin, prograde inertio-gravity ($n = 0$), mixed Rossby–gravity ($n = 0$), and Rossby ($n = 1$) waves with zonal wavenumber 1. Though inertio-gravity and mixed Rossby–gravity waves have never been observed, they are investigated together with Kelvin and Rossby waves expecting their detection in future explorations. The four waves are forced separately from below by the lower boundary condition that is described later, assuming that they are excited at lower altitudes (section 3a). The rotation rate of the coordinate system corresponds to the typical equatorial wind speed at the bottom altitude, 80 m s^{-1}.

The equations to be solved are the horizontal momentum equation, the thermodynamic energy equation, the continuity equation, and the hydrodynamic equation in the form

$$\frac{\partial u}{\partial t} = -\frac{1}{a\cos\phi}\frac{\partial u^2}{\partial \lambda} - \frac{1}{a\cos\phi}\frac{\partial (uv\cos\phi)}{\partial \phi} - \frac{\partial(\dot{\sigma}u)}{\partial \sigma} + \left(f + \frac{u\tan\phi}{a}\right)v - \frac{1}{a\cos\phi}\frac{\partial \Phi}{\partial \lambda} + X, \tag{10}$$

$$\frac{\partial v}{\partial t} = -\frac{1}{a\cos\phi}\frac{\partial (vu)}{\partial \lambda} - \frac{1}{a\cos\phi}\frac{\partial (v^2\cos\phi)}{\partial \phi} - \frac{\partial(\dot{\sigma}v)}{\partial \sigma} - \left(f + \frac{u\tan\phi}{a}\right)u - \frac{1}{a}\frac{\partial \Phi}{\partial \phi} + Y, \tag{11}$$

$$\frac{\partial T}{\partial t} = -\frac{1}{a\cos\phi}\frac{\partial (uT)}{\partial \lambda} - \frac{1}{a\cos\phi}\frac{\partial (vT\cos\phi)}{\partial \phi} - \sigma^{\kappa}\frac{\partial(\dot{\sigma}\theta)}{\partial \sigma} + \sigma^{\kappa}Q, \tag{12}$$

$$\frac{1}{a\cos\phi}\frac{\partial u}{\partial \lambda} + \frac{1}{a\cos\phi}\frac{\partial (v\cos\phi)}{\partial \phi} + \frac{\partial \dot{\sigma}}{\partial \sigma} = 0, \quad \text{and} \tag{13}$$

$$\frac{\partial \Phi}{\partial \sigma} + \frac{p_s}{\rho} = 0. \tag{14}$$

Here $\sigma \equiv p/p_s$ is the vertical coordinate, where p is the pressure and p_s is the pressure at the lower boundary; $\dot{\sigma} \equiv d\sigma/dt$ is the vertical velocity in the σ coordinate; λ is the longitude; Φ is the geopotential; T is the temperature; both X and Y represent eddy viscosity and the mechanical damping in the sponge layer; and Q represents eddy diffusivity, Newtonian cooling, and the thermal damping in the sponge layer. The equations above are finite differenced with a staggered vertical

grid system, in which variables, except for $\dot{\sigma}$, are computed at the same level and $\dot{\sigma}$ is computed at a half-grid level above and below, and a staggered horizontal grid system (grid C) described by Haltiner and Williams (1980, section 7-2, 3, 4). At the pole, variables T, Φ, and $\dot{\sigma}$ are calculated and u is zero according to its definition. Equations (10)–(12) are integrated using a centered flux-form space difference, Euler backward (Matsuno) scheme until a steady state is achieved, with (13) and (14) being used at each time step to diagnose $\dot{\sigma}$ with upper boundary condition and Φ with lower boundary condition, respectively (Haltiner and Williams 1980). The grid intervals are 22.5°, 6°, and ~0.4 km in longitude, latitude, and altitude, respectively. Though the longitudinal grid interval becomes small near the poles, with a time step of 300 s, the integration is stable and no smoothing operation is needed. The ratio of the minimum horizontal grid interval to the time step is ~410 m s^{-1}, which is much larger than the wind speed in the model; thus, the CFL condition is satisfied. The performance of the model was tested by reproducing classical wave solutions with weak forcing in zero background shear.

Since the development of the background atmosphere is beyond the scope of this study, $\overline{u}$ and $\overline{T}$ are fixed to their basic states: the variables are divided into zonal-mean and disturbance, and the former is set to be zero at each time step. The $\overline{u}$ in the nominal model (Fig. 2) is given by a simple analytic function and is barotropically and inertially stable. The location and magnitude of midlatitude jets are basically consistent with observations (e.g., Schubert 1983), although the jets are weakened near the lower boundary so that waves are smoothly introduced into the model domain. The $\overline{T}$ is the sum of an analytic function of z (Fig. 3) taken from Schubert and Walterscheid (1984) and a small correction (<25 K), which ensures thermal wind balance. The zonal-mean geopotential at the lower boundary is determined from $\overline{u}$ through cyclostrophic balance and constant with time. The meridional circulation is set to be zero.

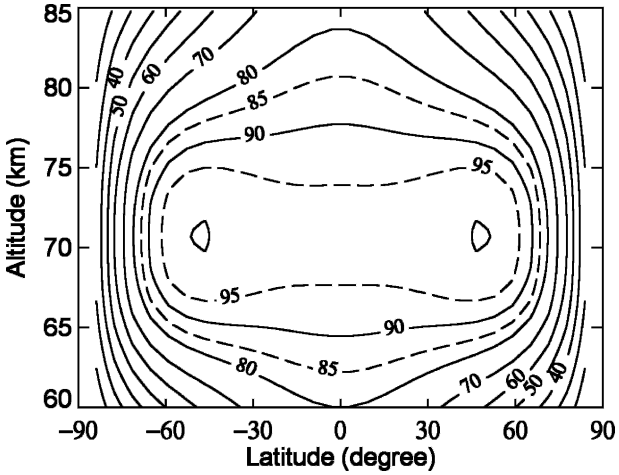

FIG. 2. Basic zonal wind distribution in the Venusian atmosphere relative to the ground surface in the nominal model.

Although the feedback to the background atmosphere is not considered, the nonlinear model includes terms of second order with respect to wave amplitude. Since the wind amplitudes of observed waves are within the same order of magnitude as their phase velocities (Rossow et al. 1990), nonlinear terms are potentially important. It is desirable to include nonlinear terms in order to confirm those terms do not hinder wave propagation. The effect of meridional circulation, which is neglected in this study, is considered to be third order or smaller. Though convective adjustment scheme is implemented, convective instability does not occur in the present experiments.

Two sets of test runs are also performed to examine the roles of the midlatitude jet and the equatorial superrotation by modifying $\overline{u}$. The $\overline{u}$ in test 1 (Fig. 4a) is a rigid-body rotation at each altitude and identical to the nominal wind profile at the equator. The $\overline{u}$ in test 2 (Fig. 4b) is the midlatitude jet component of the nominal wind (viewed from the superrotating coordinate system), and has no vertical shear at the equator.

The lower boundary conditions are given by

$$\frac{\partial u'}{\partial \sigma} = \frac{\partial v'}{\partial \sigma} = \frac{\partial T'}{\partial \sigma} = 0, \tag{15}$$

$$\Phi' = \begin{cases} \hat{\Phi} \exp\left(-\dfrac{y^2}{2l_E^2}\right) & \text{for Kelvin wave,} \\ \hat{\Phi} \dfrac{y}{l_E} \exp\left(-\dfrac{y^2}{2l_E^2}\right) & \text{for inertio-gravity and Rossby-gravity wave,} \\ \hat{\Phi}\left[\dfrac{\omega^*}{\beta\lambda^2 k}\left(1-\dfrac{y^2}{l_E^2}\right)-\dfrac{y^2}{l_E^2}\right] \exp\left(-\dfrac{y^2}{2l_E^2}\right) & \text{for Rossby wave,} \end{cases} \tag{16}$$

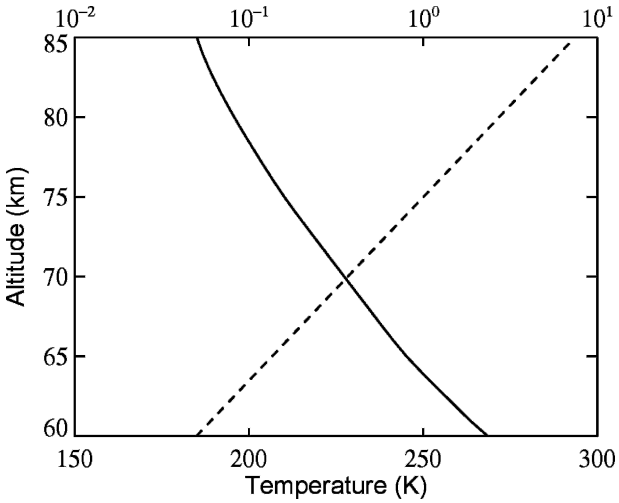

FIG. 3. Profiles of basic temperature (solid) and Newtonian cooling coefficient (dashed) in the Venusian atmosphere adopted in the model.

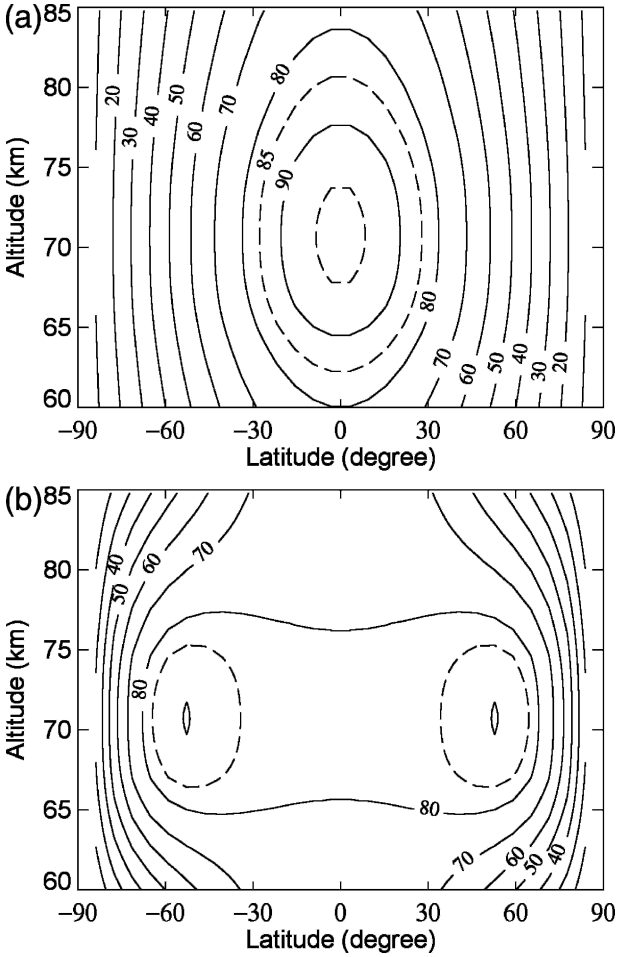

FIG. 4. Same as in Fig. 2, but for (a) test 1 and (b) test 2.

where (16) is the equatorial wave solution, with y being the northward distance from the equator, and $\hat{\Phi}$ being the amplitude scale. The l_E above is 2500, 2500, 2300, and 2200 km (~24°, 24°, 22°, and 21° in latitude) for Kelvin, inertio-gravity, Rossby–gravity, and Rossby waves, respectively. Given those values the periods of the Kelvin and Rossby waves in the inertial frame are 4.1 and 6.0 d, respectively, which are within the observed values. For inertio-gravity and mixed Rossby–gravity waves that have not been detected, we tentatively assume l_E similar to those of the Kelvin and Rossby waves. The amplitudes are given so that the wind amplitudes in the model domain become up to 5–10 m s^{-1} (Rossow et al. 1990). The parameters given and the amplitudes of induced u', v', and T' at the lower boundary are summarized in Table 1. The u' amplitude of the Rossby wave exceeds the intrinsic phase speed at the bottom, implying that the forcing is in nonlinear regime; however, the wave creates reversed potential vorticity gradient only within 1.5 km from the bottom, and the wave field near the bottom is not disturbed by higher-wavenumber components caused by barotropic instability. At the upper boundary, we impose

$$u' = v' = T' = \dot{\sigma}' = 0. \tag{17}$$

High altitudes near the upper boundary comprise a sponge layer with the damping rate given by $3 \times \exp[(z - 85)/2]$ (d^{-1}) with z scaled in kilometers, which enforces radiation condition by absorbing waves.

The eddy diffusion coefficients for momentum and heat are taken to be identical and given by 0.5 m^2 s^{-1} at all altitudes. Radio scintillation results provided coefficients of 4 m^2 s^{-1} at 60 km altitude and 0.2 m^2 s^{-1} at 45 km (Woo and Ishimaru 1981; Woo et al. 1982); however, the scintillations may not be caused by turbulence but by gravity waves (Leroy and Ingersoll 1996). The adopted value would be reasonable given such uncertainty. Radiative relaxation toward the basic state is given by Newtonian cooling with the rate coefficient shown in Fig. 3, which is roughly consistent with the calculation by Crisp (1989).

c. Results

Figure 5 shows the horizontal structures of the waves at 65 km, that is, the cloud top level. The structures of the Kelvin and Rossby waves are in agreement with observations (section 3a) if planetary-scale brightness features reflect the geopotential field. Most of the wave energy remains in each mode forced at the bottom, in

TABLE 1. Parameters of the waves forced at the lower boundary; l_E is the equatorial deformation radius, $2\pi/\omega$ is the period in the inertial frame, c^* is the intrinsic phase velocity at the equator, $\hat{\Phi}$ is the amplitude of geopotential (see text), and $\hat{u}$, $\hat{v}$, and $\hat{T}$ are the peak amplitudes of u', v', and T' at the lower boundary induced by the geopotential forcing.

Mode	l_E (km)	$2\pi/\omega$ (d)	c^* (m s^{-1})	$\hat{\Phi}$ (m^2 s^{-2})	$\hat{u}$, $\hat{v}$ (m s^{-1})	$\hat{T}$ (K)
Kelvin	2500	4.1	27	250	10, 1.6	4.7
Inertio-gravity	2500	2.7	81	250	4.9, 7.8	3.0
Rossby-gravity	2300	−15	−50	250	5.7, 10.2	1.7
Rossby	2200	−6.0	−6.8	250	8.5, 2.8	2.7

spite of the fact that the vertical scale of the background shear is not much larger than the vertical wavelengths of the waves around 65 km, which are ~8, ~7, ~20, and >20 km for the Kelvin, inertio-gravity, mixed Rossby–gravity, and Rossby waves, respectively. The latitudinal scales of the Kelvin and inertio-gravity waves are similar to their theoretical l_E of 17° and 19°, respectively, which are based on the equatorial superrotation rate at this altitude. On the other hand, the latitudinal scales of the mixed Rossby–gravity and Rossby waves are much larger than their theoretical l_E of 34° and 33°, respectively. This is attributed to the faster zonal wind in the midlatitude where the waves have most of their energy.

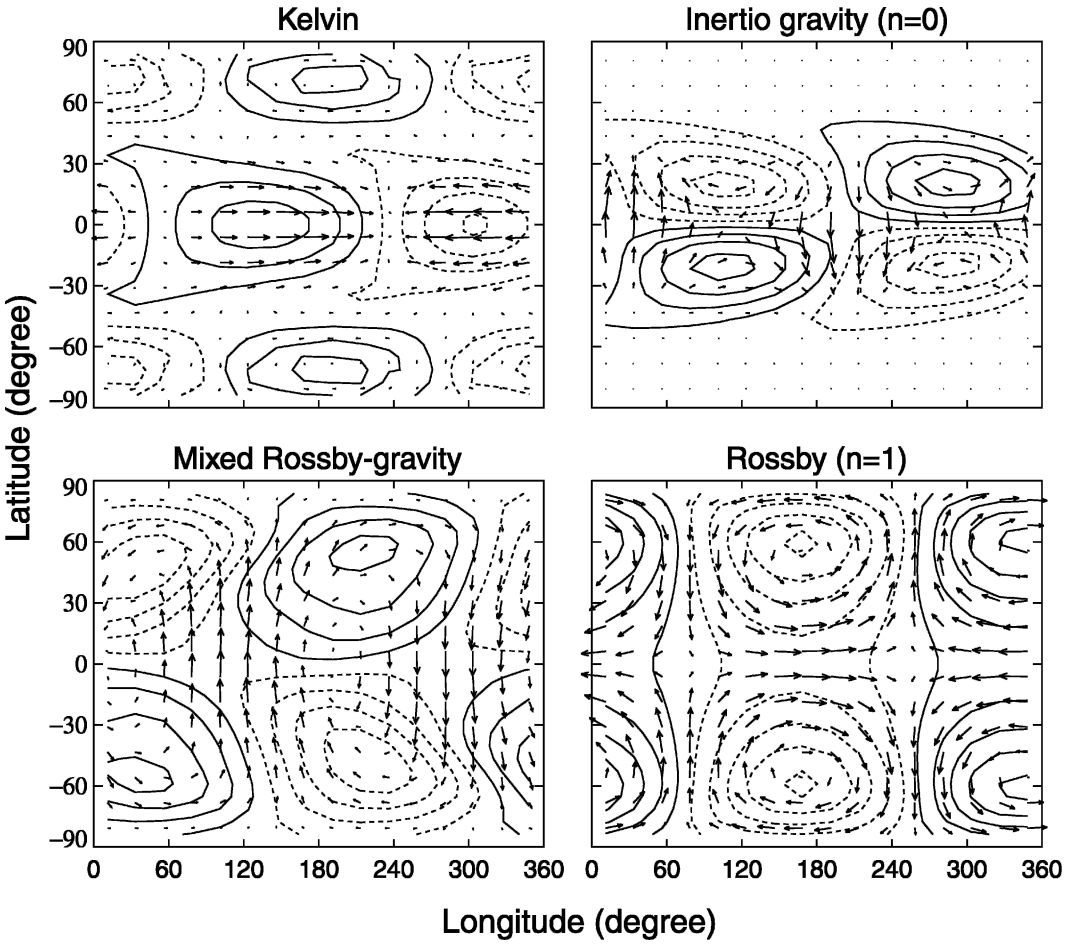

FIG. 5. Horizontal structures of the waves at 65-km altitude in the nominal model. Contours represent the disturbance geopotential with solid (dashed) contours for positive (negative) values and the contour intervals of 40, 40, 40, and 120 m^2 s^{-2} for Kelvin, inertio-gravity, Rossby–gravity, and Rossby waves, respectively. Arrows represent the disturbance horizontal wind, that are scaled so that the distance occupied by 10° represents 3.1, 7.5, 3.6, and 2.8 m s^{-1} for the respective waves. The direction of planetary rotation is from left to right.

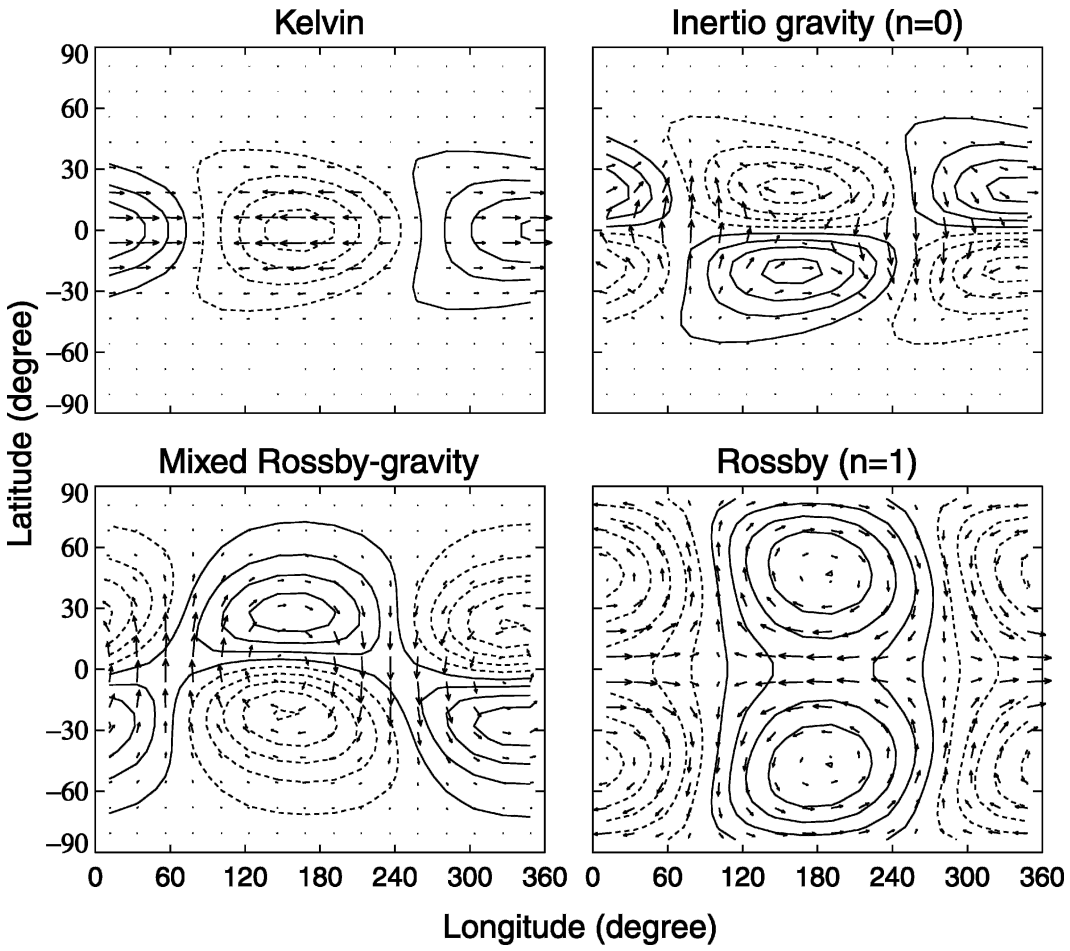

FIG. 6. Same as in Fig. 5, but for test 1. Contour interval is 40 $m^2 s^{-2}$ for all waves. Arrows are scaled so that the distance occupied by 10° represents 3.9, 8.9, 11.0, and 5.0 m s^{-1} for the respective waves.

Local maxima of geopotential are seen in the high latitude of Kelvin wave panel (Fig. 5). They move with the forcing at the bottom, and have Rossby wave–like structures with negative intrinsic phase velocities by virtue of the midlatitude jet. As shown in Fig. 6, these features disappear in test 2, in which $\bar{u}$ is rigid-body rotation at each altitude. The phase tilt with latitude in the Kelvin and Rossby wave panels in test 2 is similar to those in the Kelvin and Rossby wave solutions obtained by Covey and Schubert (1982), who considered a Venus-like atmosphere with rigid-body rotation at each altitude. Their solutions seem to reflect the influence of background vertical shear discussed in the present study.

The distributions of EP flux vectors (Fig. 7) are in agreement with the prediction: prograde waves tend to have downward and poleward EP fluxes, while retrograde waves have upward and poleward EP fluxes, in the positive vertical shear region below 70 km altitude. Above that altitude the vectors for the retrograde waves converge due to the negative vertical shear. The magnitudes of the fluxes decrease with height due to radiative damping and eddy viscosity. The EP flux divergence

$$\nabla \cdot \mathbf{F} \equiv \frac{1}{a\cos\phi}\frac{\partial}{\partial\phi}\left(F^{(\phi)}\cos\phi\right) + \frac{\partial F^{(z)}}{\partial z} \qquad (18)$$

is also plotted in the figure, indicating that prograde waves cause divergence near the equator and retrograde waves cause convergence at middle and high latitudes. Mean-wind acceleration ($d\bar{u}/dt$) is the value plotted in Fig. 7 divided by $\sigma\cos\phi$. The acceleration by the Kelvin wave and the deceleration by the Rossby wave are up to 0.3 and 0.15 m s^{-1} d^{-1}, respectively, near the cloud top (65–70 km), and the deceleration by the Rossby wave reaches maximum of 1.0 m s^{-1} d^{-1} at 75 km altitude. The deceleration by the Rossby wave will partly contribute to the driving of the meridional circulation in the mesosphere (Imamura 1997). The Kelvin

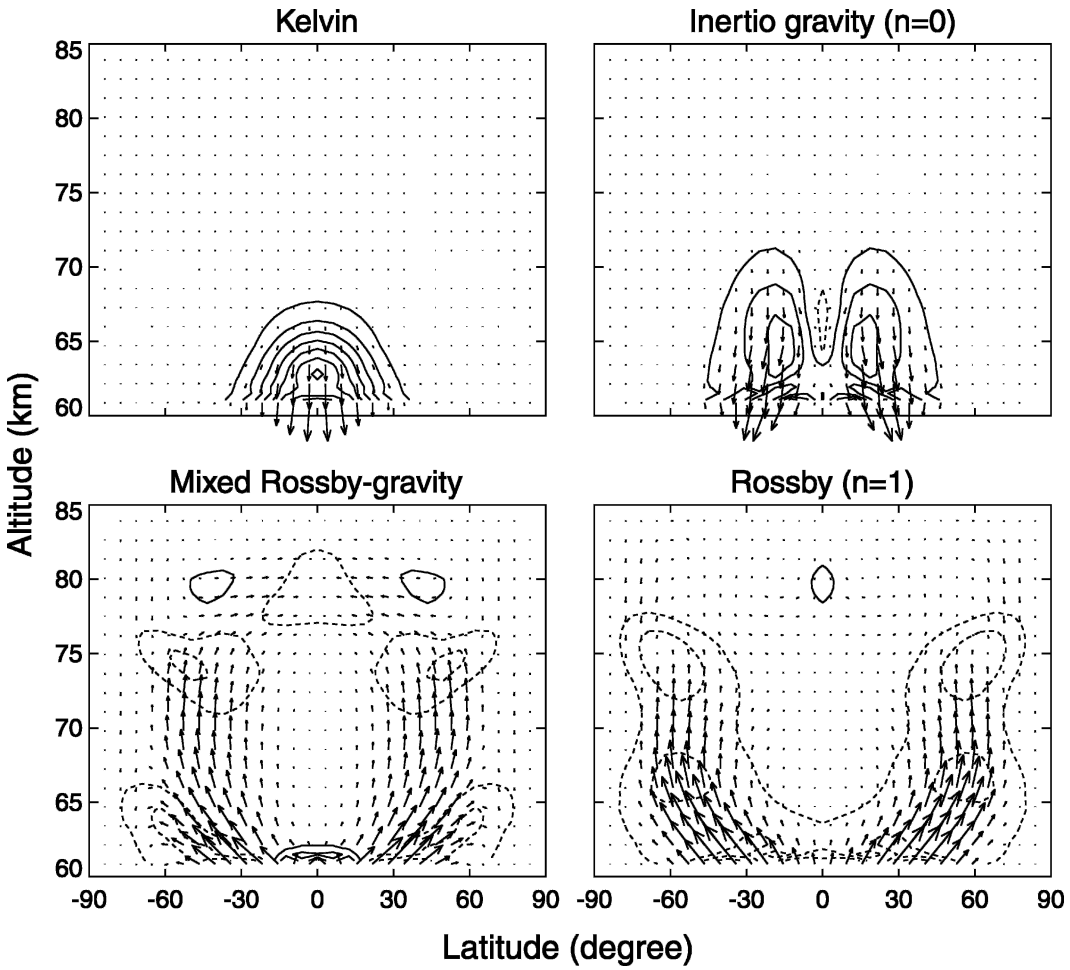

FIG. 7. Meridional distributions of EP flux vectors and their divergences for the waves in the nominal model. Arrows are scaled such that the distance occupied by 10° in ϕ represents a value $\alpha\rho_s a$ of $F^{(\phi)}$ and that occupied by 10 km in z represents a value $0.0095\alpha\rho_s a$ of $F^{(z)}$, where ρ_s is the basic density at the bottom boundary and α is 4.1, 1.5, 1.5, and 2.3 $m^2 s^{-2}$ for Kelvin, inertio-gravity, Rossby–gravity, and Rossby waves, respectively. Contours represent $(\rho_s a)^{-1} \nabla \cdot \mathbf{F}$ with solid (dashed) contours for positive (negative) values and the contour intervals of 0.03, 0.015, 0.01, and 0.01 $m\,s^{-1}\,d^{-1}$ for the respective waves.

and Rossby waves carry comparative amount of angular momentum to different latitude regions. For example, the total angular-momentum deposition by the Kelvin wave above 62 km altitude in the latitude region $|\phi| < 30°$ divided by aM, where M is the atmospheric mass in this region, is 0.11 $m\,s^{-1}\,d^{-1}$, while that by the Rossby wave in $|\phi| > 30°$ is -0.05 $m\,s^{-1}\,d^{-1}$.

Figure 8 shows the distribution of the quasigeostrophic refractive index $n^2_{k,\omega}$ (section 2b) for the Rossby wave, in which $n^2_{k,\omega}$ has maxima at ~70° due to the latitudinal curvature of $\bar{u}$. The mixed Rossby–gravity wave has a qualitatively similar $n^2_{k,\omega}$ distribution. Let the velocity scale of the wave $U = 10$ $m\,s^{-1}$, the length scale $L = a$, and the rotation rate of the coordinate system $\Omega = (80\ m\,s^{-1})/a$, and the Rossby number $U/\Omega L$ be = 1/8; thus, quasigeostrophic dynamics is potentially important in the middle and high latitude. However, the expected poleward bending of EP flux vectors near the maxima of $n^2_{k,\omega}$ is not prominent in either Rossby–gravity or Rossby wave panels (Fig. 7), except the occurrence of horizontally inclined small vectors at high latitudes. The bulk of the wave energy seems to propagate upward irrespective of such $n^2_{k,\omega}$ structure.

Figures 9 and 10 show the results of different background winds. In test 1, where $\bar{u}$ is rigid-body rotation at each altitude, the equatorward focusing of prograde waves is little changed from that in the nominal model, while the poleward expansion of retrograde waves is greatly suppressed. In test 2, where $\bar{u}$ is the midlatitude jet component of the nominal wind, the equatorward focusing of prograde waves is greatly weakened, while the poleward expansion of retrograde waves is still sig-

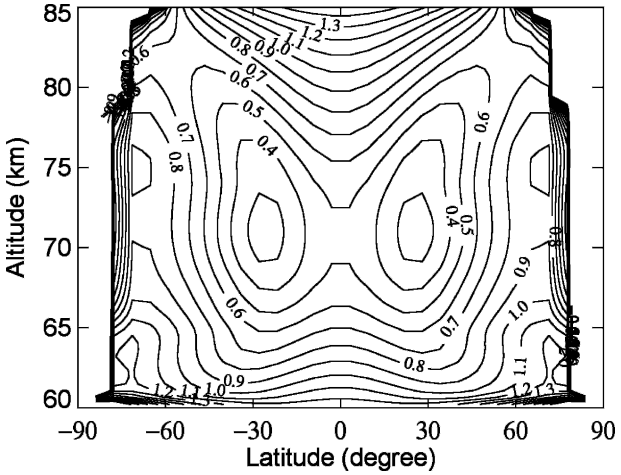

FIG. 8. Meridional distribution of the quasigeostrophic refractive index in the unit of $\log_{10}(a^2 n_{k,\omega}^2)$ for the Rossby wave in the nominal model. Regions of negative values near the poles are not plotted.

nificant. The results indicate that (i) the focusing of prograde waves in the nominal model is attributed primarily to the vertical shear of the equatorial superrotation, and (ii) the poleward expansion of retrograde waves is primarily due to the vertical shear beneath the midlatitude jets. The latter implies that planetary-scale waves "feel" the localized shear in the midlatitude.

The local deceleration near the equator in the inertio-gravity wave panel, the accelerations near the poles and in the midlatitude of ~80 km in the Rossby–gravity wave panel, and the acceleration near the equator of ~80 km in the Rossby wave panel (Figs. 7, 9, and 10) are consistent with the suggestion by Andrews and McIntyre (1976b). They studied the momentum deposition by dissipating waves and showed complex $\nabla \cdot \mathbf{F}$ distribution in which both positive and negative values occur. Considering steady waves, the EP flux divergence is related to X', Y', and Q' as (Andrews and McIntyre 1978)

$$\frac{1}{\rho_0 \cos\phi} \nabla \cdot \mathbf{F} \sim \frac{1}{a \cos^2\phi} (\overline{\eta' X'} \cos^2\phi)_\phi + (\overline{p^l X'})_p + \frac{1}{a \cos\phi} \left[\overline{\xi'_\lambda X'} + \overline{\eta'_\lambda Y'} - \frac{R}{p} \left(\frac{p}{p_s} \right)^\kappa \overline{p^l_\lambda q'} \right] - \frac{\overline{u}_p}{a \cos\phi} \left(\frac{\overline{\eta' Q'} \cos\phi}{\overline{\theta}_p} \right)_\phi - \left[f - \frac{(\overline{u} \cos\phi)_\phi}{\cos\phi} \right] \left(\frac{\overline{\eta' Q'}}{\overline{\theta}_p} \right)_p, \quad (19)$$

where particle displacements (ξ', η', p^l) and q' are defined such that

$$\left(\frac{\partial}{\partial t} + \frac{\overline{u}}{a \cos\phi} \frac{\partial}{\partial \lambda} \right) (\xi', \eta', p^l, q') = (u^l, v', \omega', Q'), \quad (20)$$

$$u^l = u' + a^{-1} \overline{u}_\phi \eta' + \overline{u}_p p^l, \quad \text{and} \quad (21)$$

$$q^l = \theta' + a^{-1} \overline{\theta}_\phi \eta' + \overline{\theta}_p p^l, \quad (22)$$

with ω' being the disturbance vertical velocity in pressure coordinate. Rough estimates of (19) with the model result showed that the $\nabla \cdot \mathbf{F}$ structure in the model is theoretically reasonable. The local deceleration near the equator in the inertio-gravity wave panel is attributed to the first term on the rhs of (19), where X' is provided by eddy viscosity. The local accelerations in the Rossby–gravity wave panel are attributed to the last term on the rhs of (19), which is nonzero due to the Newtonian cooling Q', the phase tilt with latitude, which causes equatorward EP fluxes in this region, and the amplitude variation with height. The local acceleration in the Rossby wave panel is due to the first term on the rhs of (19), where X' is from the sponge layer. Though the sponge layer is an artificial damping only for numerical experiment, eddy viscosity will take the place of sponge layer if eddy diffusion coefficient is significantly large in the upper atmosphere. When $X' = Y' = 0$ and the phase is constant with latitude, only the third term on the rhs of (19) is important and $\nabla \cdot \mathbf{F}$ is positive (negative) everywhere for prograde (retrograde) waves.

The localized divergences near the lower boundary in the mixed Rossby–gravity wave panel are attributed to the fact that the forcing (16) is not the normal mode in the sheared background, and other types of waves are also included in the forcing function. Those false waves, however, do not seem to propagate away from the lower boundary, and the EP fluxes that cause decelerations in the upper atmosphere do not originate from the divergences near the bottom but come directly from the lower boundary.

4. Conclusions

a. Wave structures in sheared flows

The present study showed that internal planetary-scale waves inherently propagate latitudinally in verti-

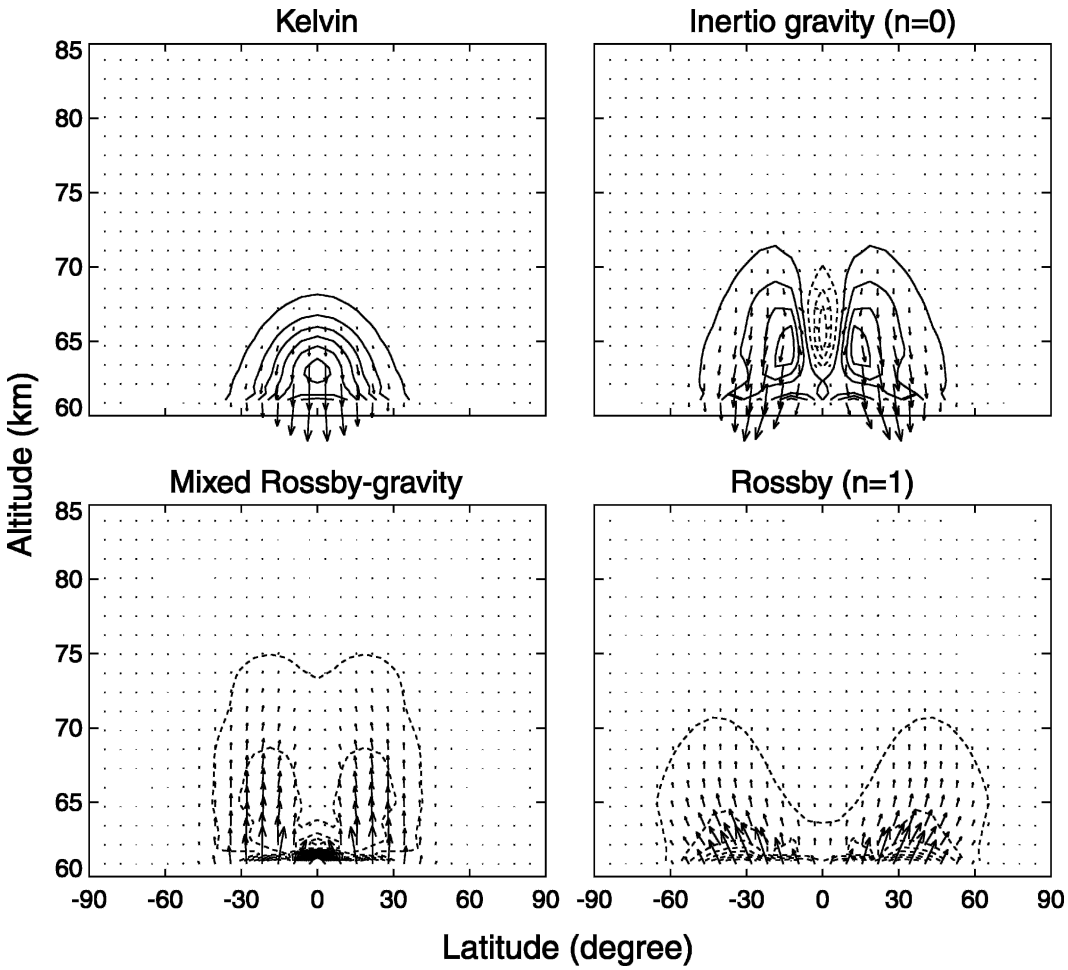

FIG. 9. Same as in Fig. 7, but for test 1. The α is 4.0, 1.5, 1.4, and 1.1 $m^2 s^{-2}$ for Kelvin, inertio-gravity, Rossby–gravity, and Rossby waves, respectively.

cal shear and cause separation of angular momentum in latitude. Because of the dependence of the wave's latitudinal scale on the intrinsic phase speed, positive (negative) vertical shear forces prograde (retrograde) waves to focus equatorward and retrograde (prograde) waves to expand poleward in the course of upward propagation. Consequently, EP flux vectors are tilted from vertical and nonzero latitudinal momentum fluxes occur. The direction of momentum transport should always be equatorward (poleward) in positive (negative) vertical shear irrespective of the zonal propagation direction. The latitudinal curvature of zonal wind will also influence the meridional propagation of retrograde waves with small Rossby number: strong midlatitude jets create maxima of the quasigeostrophic refractive index at high latitudes, thereby deflecting upwardly propagating waves poleward.

The properties mentioned above were examined with numerical solutions of Kelvin, prograde inertio-gravity, mixed Rossby–gravity, and Rossby waves in the Venusian middle atmosphere. The waves were forced separately from below, based on the characteristics of the Kelvin and Rossby waves observed at the cloud top. The results show the equatorward focusing of prograde waves and the poleward expansion of retrograde waves (Fig. 7). The former is attributed primarily to the vertical shear of the superrotation, while the latter to the vertical shear beneath the midlatitude jets. The effect of latitudinal shear seems to be minor at least for the wave parameters adopted, although small EP flux vectors directed horizontally poleward near the maxima of the refractive index were observed in the solution. The result explains why the equatorial region of the Venusian cloud top is dominated by prograde (Kelvin) waves and the high latitude is dominated by retrograde (Rossby) waves. Since the waves eventually dissipate through radiative relaxation and turbulent viscosity after meridional propagation, equatorial regions tend to

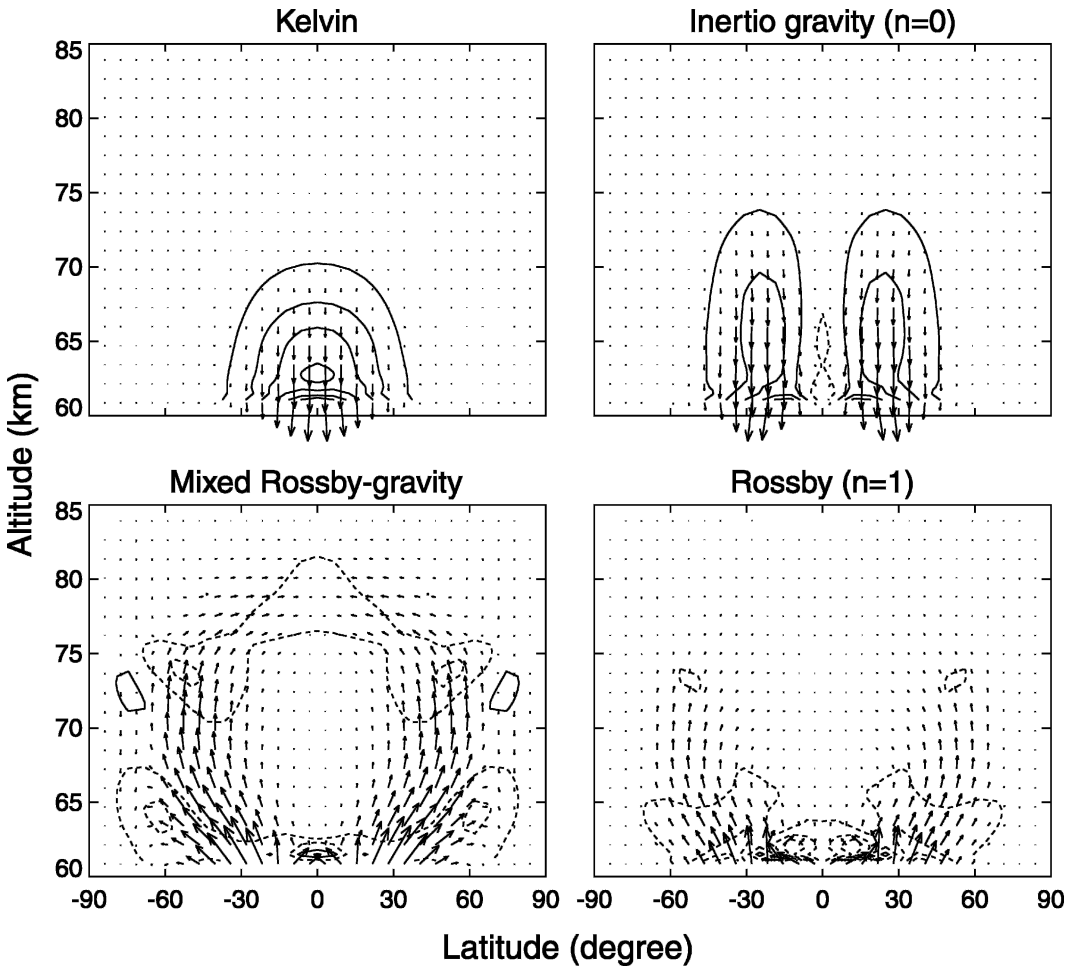

FIG. 10. Same as in Fig. 7, but for test 2. The α is 4.0, 1.5, 1.2, and 1.3 $m^2 s^{-2}$ for Kelvin, inertio-gravity, Rossby–gravity, and Rossby waves, respectively.

be accelerated and high latitudes tend to be decelerated.

The findings of this study explain some of the previous model results of the Venusian middle atmosphere dynamics. The geopotential fields of the Kelvin and Rossby waves obtained as preferred modes by Covey and Schubert (1982) show phase tilt with latitude, which resemble those seen in the present study (Fig. 6). The phase tilt in the Rossby wave implies equatorward momentum flux via $\overline{u'v'}$. Smith et al. (1993) also obtained a Kelvin-like wave as a preferred mode that causes equatorward momentum transport, being consistent with the present study. In the Venus-like GCM by Yamamoto and Takahashi (2003a), Rossby and Rossby–gravity waves with wavenumber 1–2 and gravity waves with wavenumbers 3–7 were observed and contribute to the equatorward momentum transport. The phase velocities of the waves contributing to the momentum transport scatter from -50 to 100 $m s^{-1}$ relative to the ground; on the other hand, in another Venus-like GCM with higher resolution (Yamamoto and Takahashi 2003b), the phase velocities cluster around 120–150 $m s^{-1}$ in the low latitude and 0–10 $m s^{-1}$ near the poles. Such a separation of wave modes in latitude, depending on their phase velocities, will be attributed to the influence of vertical shear discussed in this paper.

Recently near-infrared imaging techniques have been developed to observe the horizontal distributions and motions of the middle and lower clouds of Venus (e.g., Taylor et al. 1997). With such observations, combined with traditional cloud-top ultraviolet imaging, we can constrain the three-dimensional structures of planetary-scale waves to examine the present scenario. Ongoing spacecraft missions, such as the Venus Express of the European Space Agency and the Venus Climate Orbiter (PLANET-C) of Japan, will provide such observational clues.

b. Implication for the Venusian superrotation

Gierasch (1975) argued that the superrotation can be maintained by the combination of a Hadley circulation and equatorward eddy momentum flux: a Hadley circulation transports angular momentum upward when equatorial regions of the atmosphere have angular momentum surplus relative to polar regions. The occurrence of a Hadley circulation that extends to high latitudes near the cloud top is suggested by cloud motions (e.g., Rossow et al. 1990), although the cloud motions on the dayside may reflect basically thermal tides (Newman and Leovy 1992; Takagi and Matsuda 2005). The extension of the circulation down to the subcloud region is suggested by composition measurements (Collard et al. 1993). However, the mechanism of the equatorward momentum transport is unclear. Candidates include the tendency of two-dimensional motions to approach rigid body rotation (Rossow and Williams 1979), barotropic instability of midlatitude jets (e.g., Del Genio and Rossow 1990), thermal tides near the cloud top (Newman and Leovy 1992; Yamamoto and Takahashi 2004), and planetary-scale waves modified by the meridional circulation (Imamura et al. 2004).

The present study proposes another possibility for the equatorward momentum transport. Any transience due to instabilities will generate both prograde and retrograde waves, which transport momentum differently in the meridional plane. For example, the Rossby wave observed at the cloud top (section 3a) transports angular momentum downward and equatorward from the high-latitude upper atmosphere to the source region where the wave is excited, while the Kelvin wave transports angular momentum upward and equatorward from the source region to the equatorial upper atmosphere. The combination of them brings about a redistribution of angular momentum from high to low latitudes. In other words, the background shear selectively allows prograde eddy momentum to penetrate the equatorial upper atmosphere and allows retrograde eddy momentum to penetrate the polar upper atmosphere: such filtering brings about a separation of angular momentum between high and low latitudes. The estimated EP flux divergence near the equator is comparable to the equatorial acceleration required to maintain the superrotation, which is estimated to be ~ 0.5 m s^{-1} d^{-1} (Newman and Leovy 1992). It is possible that only the equatorial acceleration by prograde waves is important and the deceleration by retrograde waves at high latitudes is unnecessary; however, if both prograde and retrograde waves are excited and propagate upward in the same latitude region, the net mean acceleration may become small similarly to the classical theory of the quasibiennial oscillation in the terrestrial stratosphere. The poleward emanation of retrograde waves prevents such momentum cancellation.

It should be stressed that midlatitude jets might play more important role than equatorial superrotation in modifying the direction of EP fluxes in many cases. Even if the atmospheric region under consideration does not have background shear in its initial condition, midlatitude jets will be created at upper levels by the poleward advection of absolute angular momentum in the Hadley circulation. More work is needed to examine the process in various conditions.

Acknowledgments. The author would like to thank two anonymous reviewers and Dr. G. Schubert for carefully reading the manuscript and making constructive suggestions.

REFERENCES

Andrews, D. G., and M. E. McIntyre, 1976a: Planetary waves in horizontal and vertical shear: Asymptotic theory for equatorial waves in weak shear. *J. Atmos. Sci.,* **33,** 2049–2053.

——, and ——, 1976b: Planetary waves in horizontal and vertical shear: The generalized Eliassen–Palm relation and the mean zonal acceleration. *J. Atmos. Sci.,* **33,** 2031–2048.

——, and ——, 1978: Generalized Eliassen–Palm and Charney–Drazin theorems for waves on axisymmetric mean flows in compressible atmospheres. *J. Atmos. Sci.,* **35,** 175–185.

——, J. R. Holton, and C. B. Loevy, 1987: *Middle Atmosphere Dynamics.* Academic Press, 150 pp.

Chen, P., and W. A. Robinson, 1992: Propagation of planetary waves between the troposphere and stratosphere. *J. Atmos. Sci.,* **49,** 2533–2545.

Collard, A. D., and Coauthors, 1993: Latitudinal distributions of carbon monoxide in the deep atmosphere of Venus. *Planet. Space Sci.,* **41,** 487–494.

Covey, C., and G. Schubert, 1982: Planetary-scale waves in the Venus atmosphere. *J. Atmos. Sci.,* **39,** 2397–2413.

Crisp, D., 1989: Radiative forcing of the Venus mesosphere II. Thermal fluxes, cooling rates, and radiative equilibrium temperatures. *Icarus,* **77,** 391–413.

Del Genio, A. D., and W. B. Rossow, 1990: Planetary-scale waves and the cyclic nature of cloud top dynamics on Venus. *J. Atmos. Sci.,* **47,** 293–318.

Forbes, J. M., 2002: Wave coupling in terrestrial planetary atmospheres. *Atmospheres in the Solar System: Comparative Aeronomy, Geophys. Monogr.,* Vol. 130, Amer. Geophys. Union, 171–190.

Gierasch, P. J., 1975: Meridional circulation and the maintenance of the Venus atmospheric rotation. *J. Atmos. Sci.,* **32,** 1038–1044.

Haltiner, G. J., and R. T. Williams, 1980: *Numerical Prediction and Dynamic Meteorology.* 2d ed. John Wiley & Sons, 477 pp.

Holton, J. R., 1970: The influence of mean wind shear on the propagation of Kelvin waves. *Tellus,* **22,** 186–193.

Imamura, T., 1997: Momentum balance of the Venusian midlatitude mesosphere. *J. Geophys. Res.,* **102,** 6615–6620.

——, T. Horinouchi, and T. J. Dunkerton, 2004: The lateral trans-

port of zonal momentum due to Kelvin waves in a meridional circulation. *J. Atmos. Sci.,* **61,** 1966–1975.

Leroy, S. S., and A. P. Ingersoll, 1996: Radio scintillations in Venus's atmosphere: Application of a theory of gravity wave generation. *J. Atmos. Sci.,* **53,** 1018–1028.

Lindzen, R. S., 1970: Internal equatorial planetary-scale waves in shear flow. *J. Atmos. Sci.,* **27,** 394–407.

——, 1971: Equatorial planetary waves in shear: Part I. *J. Atmos. Sci.,* **28,** 609–622.

Longuet-Higgins, M. S., 1968: The eigenfunctions of Laplace's tidal equations over the sphere. *Philos. Trans. Roy. Soc. London,* **A262,** 511–607.

Matsuno, T., 1966: Quasi-geostrophic motions in the equatorial area. *J. Meteor. Soc. Japan,* **44,** 25–43.

——, 1970: Vertical propagation of stationary planetary waves in the winter Northern Hemisphere. *J. Atmos. Sci.,* **27,** 871–883.

Newman, M., and C. B. Leovy, 1992: Maintenance of strong rotational winds in Venus' middle atmosphere by thermal tides. *Science,* **257,** 647–650.

Rossow, W. B., and G. P. Williams, 1979: Large-scale motion in the Venus stratosphere. *J. Atmos. Sci.,* **36,** 377–389.

——, A. D. Del Genio, and T. Eichler, 1990: Cloud-tracked winds from Pioneer Venus OCPP images. *J. Atmos. Sci.,* **47,** 2053–2084.

Schubert, G., 1983: General circulation and dynamical state of the Venus atmosphere. *Venus,* D. M. Hunten et al., Eds., The University of Arizona Press, 650–680.

——, and R. L. Walterscheid, 1984: Propagation of small-scale acoustic-gravity waves in the Venus atmosphere. *J. Atmos. Sci.,* **41,** 1202–1213.

Smith, M. D., P. J. Gierasch, and P. J. Schinder, 1993: Global-scale waves in the Venus atmosphere. *J. Atmos. Sci.,* **50,** 4080–4096.

Takagi, M., and Y. Matsuda, 2005: Sensitivity of thermal tides in the Venus atmosphere to basic zonal flow and Newtonian cooling. *Geophys. Res. Lett.,* **32,** L02203, doi:10.1029/2004GL022060.

Taylor, F. W., D. Crisp, and B. Bezard, 1997: Near-infrared sounding of the lower atmosphere of Venus. *Venus II*, S. W. Bougher, D. M. Hunten, and R. J. Phillips, Eds., The University of Arizona Press, 325–351.

Woo, R., and A. Ishimaru, 1981: Eddy diffusion coefficient for the atmosphere of Venus from radio scintillation measurement. *Nature,* **289,** 383–384.

——, J. W. Armstrong, and A. J. Kliore, 1982: Small-scale turbulence in the atmosphere of Venus. *Icarus,* **52,** 335–345.

Yamamoto, M., and M. Takahashi, 2003a: The fully developed superrotation simulated by a general circulation model of a Venus-like atmosphere. *J. Atmos. Sci.,* **60,** 561–574.

——, and ——, 2003b: Superrotation and equatorial waves in a T21 Venus-like AGCM. *Geophys. Res. Lett.,* **30,** 1449, doi:10.1029/2003GL016924.

——, and ——, 2004: Dynamics of Venus' superrotation: the eddy momentum transport processes newly found in a GCM. *Geophys. Res. Lett.,* **31,** L09701, doi:10.1029/2004GL019518.

Young, R. E., H. Houben, and L. Pfister, 1984: Baroclinic instability in the Venus atmosphere. *J. Atmos. Sci.,* **41,** 2310–2332.